

# EVALUATION OF UNSTEADY CFD MODELS APPLIED TO THE ANALYSIS OF A TRANSONIC HP TURBINE STAGE

*M. Giovannini*<sup>1</sup> – *M. Marconcini*<sup>1</sup> – *A. Arnone*<sup>1</sup>  
*F. Bertini*<sup>2</sup>

<sup>1</sup> Department of Industrial Engineering, University of Florence, Florence, Italy  
Matteo.Giovannini@unifi.it

<sup>2</sup>R&D, Avio Group, Rivalta di Torino, Italy  
Francesco.Bertini@aviogroup.com

## ABSTRACT

This paper presents an efficient “Phase-Lagged” method developed for turbomachinery applications. The method is based on the Generalized-Shape-Correction model. Moving averages techniques as well as double-passage domain formulation were adopted in order to reduce memory requirements and improve the model robustness. The model was used to evaluate the aerodynamic performance of the high pressure transonic turbine stage CT3, experimentally studied at the von Kármán Institute for Fluid Dynamics within the EU funded TATEF2 project. Results are discussed and compared with both the available experimental data and the results obtained by means of both steady and unsteady scaled Full-Annulus approaches. Computational requirements of the GSC model are evaluated and presented showing that nowadays unsteady results can be reached at an affordable computational cost.

## NOMENCLATURE

$c$  chord  
 $\hat{w}$  chorochronic harmonics coefficient  
 $\Delta t$  physical time step  
 $f$  frequency  
 $h$  span height  
 $j$  imaginary unit  
 $\Im$  imaginary part operator  
 $\Re$  real part operator  
 $L_\theta$  total number of nonzero harmonics  
 $N_B$  blade count  
 $N_{pt}$  total number of perturbations  
 $N_T$  number of time period  
 $N_t$  total number of time harmonics  
 $N_\theta$  total number of space harmonics  
 $Re$  Reynolds number  
 $T$  time period  
 $\tilde{w}$  time harmonics coefficient  
 $w$  generic solution variable  
 $w_0$  time-space average value  
 $t$  time  
 $v$  velocity magnitude

### Greek:

$\beta_r$  chorochronic phase shift

$\chi$  relaxation coefficient  
 $\omega$  rotational velocity

### Subscripts:

$0$  total quantities  
 $ave$  averaged  
 $i,j$  row index  
 $is$  isentropic  
 $R$  rotor  
 $ref$  reference quantities

### Acronyms:

BCs Boundary Conditions  
BDF Backward Difference Formula  
BPF Blade Passing Frequency  
FA Full-Annulus  
GSC Generalized Shape-Correction  
LE Leading Edge  
MP Mixing-Plane  
PL Phase-Lagged  
NRBC Non-Reflecting BCs  
SS Suction Side  
TE Trailing Edge

### Superscripts and oversigns:

$^{[p]}$  perturbation index

## INTRODUCTION

Nowadays, steady three-dimensional CFD is a standard design tool adopted in the turbomachinery industry even if the flow field in such machines is inherently unsteady as a result of the interaction of the rotating and stationary blade rows. Steady Mixing-Plane (MP) models have reached very high levels of confidence and accuracy with low computational costs.

Unsteady solvers have been available for a long time, nevertheless, unsteady CFD computations have not been applied as turbomachinery design tool so far. No theoretical difficulties have prevented a daily use of such techniques, rather unsteady approaches have found their major drawback in their computational costs. If standard periodic BCs are adopted the computational domain has to cover a periodic sector of the machine. Due to mechanical design constrains, in a multi-rows environment, no common divisors can be found among blade counts and the computational domain usually should cover the whole wheel (Full-Annulus (FA) approach) leading to model size several orders of magnitude bigger than that of the corresponding steady Mixing-Plane model (Hall and Ekici (2005)).

However, the importance of the introduction of unsteady computations into the design process has been asserted in several papers both for turbines and compressors (e.g. He et al. (2002); Blumenthal et al. (2011)) and it is one of the most important aspects of the current CFD codes. Therefore, great emphasis has been recently devoted in developing simplified models which ensure high accuracy and low computational costs.

In the so called “scaled-model” a geometrical (blade count) alteration of the computed geometry is enabled in order to find a small periodic sector and reduce the computational domain. If a proper scaling is adopted the main steady (time-averaged) performance can be accurately predicted. However, the fundamental frequencies of the unsteady flow are altered and poor accuracy is obtained if relevant pitch variations are adopted. Similar considerations can be made when considering the Profile Transformation approach proposed by Galpin et al. (1995), in which the actual blade geometry is not scaled, but the flow field is stretched or compressed in the rotor-stator interfaces. In this context, methods able to retain small computational domain without any geometrical alteration would be extremely valuable.

Gopinath (2007) developed a time spectral method specifically developed for time periodic problems based on the Fourier transformation of the whole computational domain. Alternatively, Giles (1988) proposed the Time Inclined approach in which a space-time transformation of the governing equation allows the solution of a single passage domain. Unfortunately, this model can be applied to single stage problems only and is affected by problematic post-processing. Moreover, starting from the first work of Adamczyk (1985), several linear and non-linear harmonic methods were developed for aeroelastic applications and blade-row interaction analyses (He and Ning (1999); Vilmin et al. (2006)). The Harmonic Balance approach is based on the model proposed by Hall and Lorence (1993) and it represents an improved time-linearized multi-stage approach for Euler and viscous flow calculations (Hall and Ekici (2005)). Finally, a relevant improvement in the attempt to reduce the computational cost of unsteady computations was obtained with the introduction of the Phase-Lagged method (PL). Starting from the pioneer work of Erdos et al. (1977) this technique introduces phase-shifted boundary conditions, thus resulting in the reduction of the computational domain to a single blade passage.

In the work reported herein, a PL model was implemented in the TRAF code, followed by a 3D unsteady CFD analysis of an high pressure transonic turbine stage. A comprehensive description of the model is given, mainly focusing on the implementation features that have allowed to overcome the main stability limits frequently reported in literature. Noteworthy, the presented test case allowed us also to evaluate both the accuracy and the computational costs of different approaches in solving complex flow field. In particular, a steady-state mixing-plane (MP), an unsteady full-annulus (FA), and a Phase-Lagged (PL) methods have been deeply investigated and evaluated assessing their memory and time requirements and comparing predicted and available experimental data.

## IMPLEMENTATION

### The TRAF code

The present work was performed using the TRAF code (Arnone (1994)). The code is a Q3D/3D multi-row, multi-block CFD solver for the RANS/URANS equations, written in conservative form in a curvilinear, body-fitted coordinate system. The steady Navier-Stokes equations are reformulated to be handled by a time marching steady-state approach. The non-reflecting boundary conditions (NRBC) proposed by Giles (1988) was adopted in the steady mixing-plane computations in order to prevent spurious, nonphysical reflections at inflow and outflow boundaries. In the time-accurate scheme, derivatives with respect to time  $t$  are discretized using a three points Backward Difference Formula (BDF) and solved by means of a dual time stepping method. The code features several turbulence closures ranging from simple algebraic model to one, two and three-equation, transition-sensitive, turbulence models (Pacciani et al. (2011)).

### The Generalized Shape-Correction model

All of the PL models are based on the chorochronic relations originally introduced by Erdos et al. (1977) and subsequently more strictly proved by Gerolymos and Chapin (1991). In a rotor-stator environment, if the natural instabilities (such as vortex shedding, rotating stall, separation bubble buffeting, etc.) are absent or almost negligible, then each blade row observes a periodic flow field in its relative frame of reference. The fundamental frequency is equal to the blade passing frequency (BPF) of the adjacent row ( $f_i$ ) and each blade passage witnesses the same phenomena of its neighbor with a phase shift ( $\beta_r$ ) that can be easily derived from kinematic considerations leading to the well known chorochronic periodicity conditions:

$$w_i(x, r, \theta, t) = w_i(x, r, \theta - \frac{2\pi}{N_{B_i}}, t + \frac{\beta_{r_i}}{2\pi f_i}) \quad (1)$$

The Shape-Correction approach was originally proposed by He (1990) for oscillating blades. It was then generalized (Generalized Shape-Correction (GSC) method) to handle multi-perturbation problems (He (1992)) and it has been applied to solve blade row interactions (Dewhurst and He (2000); Gerolymos et al. (2002)).

An advanced algorithm based on the moving-averages technique proposed by Gerolymos et al. (2002) was adopted in the implemented model in order to reduce memory requirements and improve convergence rate.

### Boundaries between blocks of the same row

A generic solution variable at a periodic boundary is expressed by means of Fourier series in time with a finite number of time-harmonic coefficients:

$$w(x, r, \theta, t) = w_0(x, r, \theta) + \sum_1^{N_{pt}} \Re \left\{ \sum_1^{N_t} \tilde{w}_p(x, r, \theta, n_t) e^{j2\pi n_t f^{[p]} t} \right\} \quad (2)$$

For single stage computations  $N_{pt} = 1$  and  $f^{[p]}$  refer to the BPF of the adjacent row. In a multi-stage environment, due to the presence of many rows in relative motion and with different blade counts, the unsteady flow field is dominated by several perturbations and one BPF can be defined for each row on the basis of simple kinematic considerations. At the time of writing, even if a general formulation has been developed, only two BPF are considered in each row as suggested by Neubauer (2004) and Van Zante et al. (2008). The interactions with the two adjacent rows are then taken into account while

other perturbations are mixed out at the inter-row interfaces.

Both moving-averages and relaxation techniques are adopted for computing Fourier coefficients<sup>1</sup>:

$$\tilde{w}_p(n_t)|_{n+1} = \tilde{w}_p(n_t)|_n + \chi_t C(n_t) \frac{1}{T} \Delta t e^{-j2\pi n_t f^{[p]} t} \left\{ w(t_{new}) - \left[ w_0 + \sum_1^{N_{pt}} \Re \left\{ \sum_1^{N_t} \tilde{w}_p(n_t) e^{j2\pi n_t f^{[p]} t} \right\} \right] \right\} \quad (3)$$

Coefficients are updated at the end of each physical time step while they are kept constant during the Runge-Kutta steps, the multigrid scheme and the sub-iterations. BCs are finally imposed in the phantom cells on one side of a given blade passage (gray cells in fig. 1(a)) by using Fourier series of the donor cells in the opposite side of the block (black cells in fig. 1(a)) with the proper time-shift:

$$w(x, r, \theta, t) = w_0(x, r, \theta \pm \frac{2\pi}{N_B}) + \sum_1^{N_{pt}} \Re \left\{ \sum_1^{N_t} \tilde{w}_p \left( x, r, \theta \pm \frac{2\pi}{N_B}, n_t \right) e^{j n_t \beta_r^{[p]}} e^{j2\pi n_t f^{[p]} t} \right\} \quad (4)$$

### Boundaries between different blade rows

The flow variables at inter-row interfaces are expressed by  $t - \theta$  Fourier series:

$$w(x, r, \theta, t) = \Re \left\{ \sum_0^{L_\theta} \hat{w}(n_t = 0, n_\theta) e^{j n_\theta \theta} \right\} + \sum_1^{N_{pt}} \Re \left\{ \sum_1^{N_t} \sum_0^{L_\theta} \hat{w}_p(n_t, n_\theta) e^{j2\pi n_t f^{[p]} t + j n_\theta \theta} \right\} \quad (5)$$

where the first term on the left side returns the time averaged spatial distribution, while the second one includes the nonzero  $t - \theta$  harmonics that satisfy the chorochronic periodicity condition (Neubauer (2004)). The Fourier coefficients are computed by inverse Fourier transformations with moving averages technique in each circle passing through donor cells of a given rows:

$$\hat{w}_p(n_t, n_\theta)|_{n+1} = \hat{w}_p(n_t, n_\theta)|_n + \chi_{t\theta} \frac{\Delta t}{2\pi T} \left[ I_\theta \left( t_{new}, f^{[p]}, n_\theta \right) - I_\theta \left( t_{old}, f^{[p]}, n_\theta \right) \right] e^{-j2\pi n_t f t_{new}} \quad (6)$$

where  $I_\theta$  is the spatial inverse Fourier transformation over the wheel (Gerolymos et al. (2002)) computed by using the current ( $new$ ) or the rebuilt ( $old$ ) solution values.

### Initialization

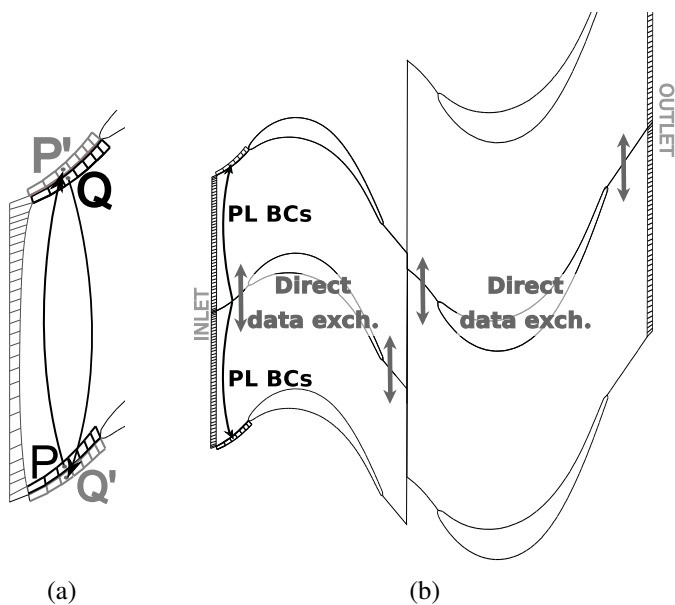
Despite the several time-consuming initialization procedures proposed in literature (Chen and Barter (1998); Barter et al. (2000)), a very simple “*constant-initialization*” is adopted in the present model, as it does not hinder the model convergence.

Steady results are used to initialize the solution variables in all the grid cells and the mean values ( $\tilde{w}_p(n_t = 0)$  and  $\hat{w}_p(n_t = 0, n_\theta = 0)$ ) of the Fourier series. All the remaining time harmonic and chorochronic harmonic coefficients are initialized to zero.

### Double passage approach

The low robustness of the Phase-Lagged models is frequently reported in literature (see Li and He (2001); Dewhurst and He (2000)). Several tests have proved that the main troubles are due to the proximity between donor and phantom cells. This feature is well highlighted in fig. 1(a) in which the boundaries in the front part of a blade passage are shown. During the initial transient of the computation the computed flow field is not periodic, the Fourier coefficients have not reached convergence and inaccurate values are set in the phantom cells ( $P'$  and  $Q'$ ) giving rise to spurious disturbances near boundaries. Moreover, these perturbed values are used in the donor cells ( $P$  and  $Q$ ) to compute Fourier transformations and to update harmonic coefficients. These spurious perturbations

<sup>1</sup>hereafter,  $(x, r, \theta, t)$  coordinates when obvious will be omitted for the sake of simplicity



<i>(Double pass.)/(Single pass.)</i>	
mem. req.	<b>2</b>
t per $T$ (serial time)	2
$N_T$ to periodic.	1/10
<b>t to periodic.</b>	<b>1/5</b>

Table 1: **Computational costs**

Figure 1: **Sketch of the computational domain: a) single passage model; b) double passage model.**

are not dumped by the numerical scheme and can corrupt the whole domain.

To overcome this problem, Biesinger et al. (2010) suggested the adoption of a two-passage model. In each row, phantom cells of one block overlap the real cells of the other at the interface between the two blade-passage, and a direct data exchange suffices to provide BCs (fig. 1(b)). In the lower and upper bound of the computational domain, instead, chorochronic boundary conditions must be used as they are non periodic interfaces.

The computational costs per time period with this approach are twice that of single-passage ones: memory usage is exactly doubled and also the computational time (in a serial approach) follows the same trend. However, the superior quality of the data used to compute the Fourier coefficients provides very high robustness to the model, so that the two passage model reaches convergence in a tenth of the time periods needed by the single passage approach. Overall, this approach results in a significantly reduced time (at least 5 times lower than the original one) thus making acceptable the extra memory usage.

### Memory requirements

Data from several real LPT modules derived from the Avio database have been taken into account in order to quantify the computational costs of the steady MP, and the unsteady FA and GSC models. As previously mentioned, the FA computational domain can be reduced from the full-annulus to a small sector if some angular periodicity can be found among all the blade rows. Due to mechanical design constrains, usually there is not any common divisor among the blade counts in actual turbomachinery configurations and periodicity is reached only over the whole wheel. However, a slight modification of the blade counts in the numerical model can lead to a favourable combination of the blade numbers and can allow a sizeable reduction of the computational domain. Since these alterations of the blade counts directly affects the blade pitch, a proper geometry transformation is needed in order to preserve the main steady row performance (Arnone and Pacciani (1996)). In the present analysis this “FA scaled” model was taken into account in assessing the computational costs of unsteady computations. In particular, three values (1, 2 and 3%) were considered for the blade pitch alteration. Computational costs were evaluated as a function of the number of rows taken into

## MEMORY REQUIREMENTS

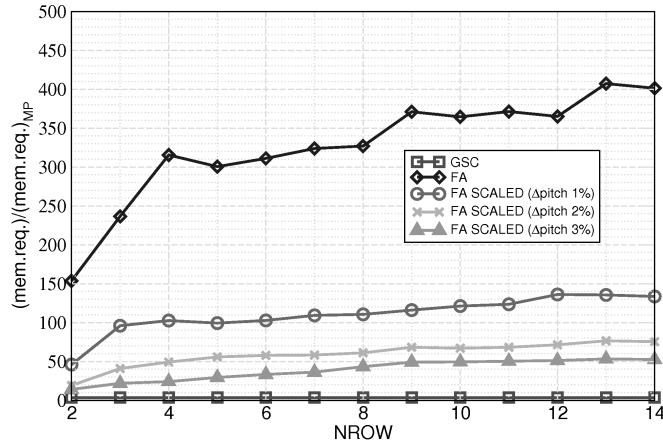


Figure 2: Memory requirements for a “mean” turbine: comparison among the FA, FA scaled (1%, 2%, 3%) and GSC approaches.

account in the computation (from the single stage to the whole machine) and plotted as the ratio between the memory requirements of a given unsteady approach and that of the MP model (fig. 2). Plotted results refer to a sort of “mean-turbine” obtained by averaging data of the real ones, being the specific information of the modules confidential. The graph clearly shows that the FA requirements grows up very rapidly, becoming two order of magnitude greater than MP ones after very few stages. Considering very few rows, the FA scaled model allows a cost reduction of an order of magnitude although this result can be reached only when considering relevant pitch variations (2, 3% or even more). Differently, the GSC memory requirements are only 2.5 times greater than the steady model ones as a reduced domain is solved and only the Fourier coefficients are stored. Furthermore these values are not affected by neither the blade counts nor the number of the solved rows.

## HIGH PRESSURE TRANSONIC TURBINE STAGE

The aforementioned CFD model was applied to the analysis of the CT3 high pressure stage experimentally investigated at the von Kármán Institute in the frame work of the TATEF2 EU funded project. Computations refer to the test facility in which the vane has been restaggered by 2 deg (Loma et al. (2007)). The turbine stage is composed by 43 uncooled cylindrical vanes and 64 uncooled twisted blades. Main geometrical features as well as the operating conditions of the measurement campaign are listed in tab. 2. Since the blade counts in the stator and the rotor rows have not any common divisor, the FA computational domain should cover the whole wheel resulting in huge computational costs. Therefore, the stage geometry was scaled considering 42 stator vanes and 63 rotor blades and a blade count ratio of 2:3 for the unsteady FA computations. This modification allowed us to compute only 1/21 of the row rings even if pitch alterations of 2.4% and 1.6% were introduced for the stator and the rotor rows respectively. A uniform temperature distribution ( $T_w = 289K$ ) was prescribed on solid walls while a value of  $Tu = 2.5\%$  was imposed at stator inlet.

The H-type grids generated for both steady and unsteady computations are shown in fig. 3. The mesh

	$c_x/h$	$pitch/c_x$	Stagger [deg]	$N_B$	$Re(10^6)$	$M_{2,is}$	$M_{3r,is}$	$p_{01}/p_{03}$	
Vane	0.81	1.313	54	43	Low	1.063	1.071	0.65	2.19
Blade	0.74	0.912	32	64	Nom	1.072	1.242	0.97	3.19
					High	1.074	1.249	1.18	3.85

Table 2: CT3: geometrical features and operating conditions (midspan).

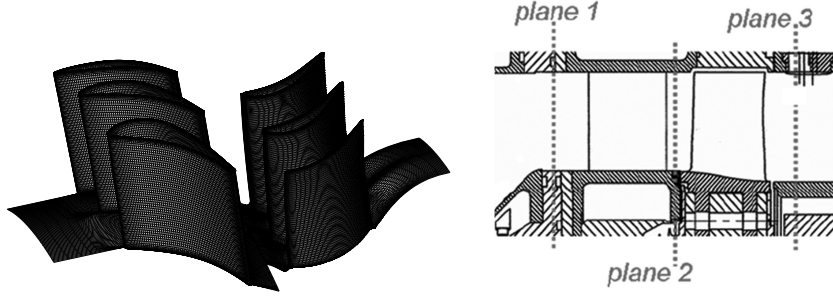


Figure 3: CT3 transonic stage mesh and axial positions of the measurement planes.

<i>Computational costs</i> (serial Intel Xeon CPU @ 2.40)					
	MP	GSC	FA	FA scaled	
mem. req.	1.1	3.1	82	3.8	[GB]
t per $T$	x	90.2	2100*	5.5	[h]
$N_T$ to periodic.	x	4	3 ~ 4*	10	[-]
t to periodic.	0.08	12	270. *	3	[day]

\* estimated

Table 3: **Computational costs of the MP, GSC, FA and FA scaled approaches.**

size ( $220 \times 100 \times 90 \approx 2 \cdot 10^6$  cells per blade passage) and the number of time and chorochronic harmonics in Fourier series ( $N_t = 10$ ,  $L_\theta = 10$ ) were selected by means of a sensitivity analysis. About 5-10 sub-iterations were computed per time step considering a switching RMS residual value of  $10^{-8}$ . The time-sampling of the unsteady computations was imposed considering a trade-off between accuracy and computational costs: computations were performed using 50, 100, and 200 time steps per blade passage resulting in 3200, 6400, and 12800 time steps on the full wheel revolution respectively. According to the second-order BDF scheme adopted for the time derivative operator, at least 16 points are needed to accurately solve a given wavelength (see Gopinath (2007)). Therefore the first 3 BPF harmonics are accurately solved even with 50 time steps, 5-6 harmonics with 100, and so on. Each unsteady computation is carried out until a periodicity condition is reached. Periodicity is evaluated by monitoring the variation over two consecutive periods of several flow quantities: mass flow rate, unsteady blade load, overall efficiency, etc.

The computational costs of both steady and unsteady approaches are reported in tab. 3. Memory requirement for the GSC model is of the same order of magnitude of the MP one and one order lower than that of the FA approach. The FA scaled model is very attractive as it provides memory requirements comparable to the GSC ones, but lower computational time. Unfortunately, these results have not general validity, as they are strictly linked to the present blade count ratio. By using the parallel version of the TRAF code implemented in a portable, scalable form for distributed-memory parallel computers using Message Passing Interface (MPI) standard for communication, the computational time was drastically reduced. Indeed GSC computation reached convergence in less than 3 days using only 4 CPUs (Intel Xeon CPU @ 2.40GHz). Unlike the FA approach, GSC performance do not depend on the test-case. Moreover, multistage domains and even whole LPT modules can be solved with similar computational costs (few days and few CPUs).

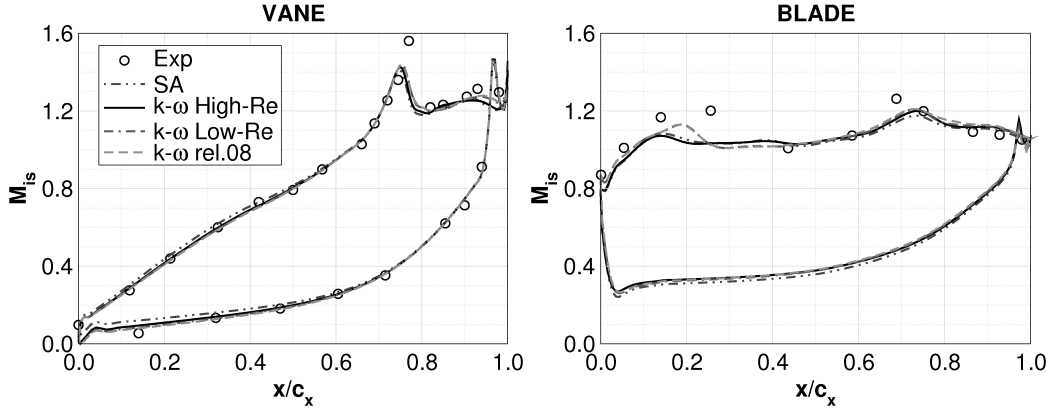


Figure 4: **Time-averaged isentropic Mach number distribution (GSC model, *Nom*-condition 50% span). Comparison among different turbulence models: Spalart and Allmaras (1994) (SA),  $k - \omega$  Wilcox (1998) low/high Reynolds vers., and  $k - \omega$  Wilcox (2008).**

## Results

### Turbulence model

The proper turbulence model was selected on the basis of a first sensitivity analysis. Fig. 4 shows a comparison of the time-averaged isentropic Mach number distribution obtained with different turbulence models. As can be seen a different behaviour of the flow field was predicted in the rear part of the vane and in front part of the blade, where, the shock-boundary layer interaction is of major concern. More exactly, a separation bubble was predicted in both the stator and the rotor suction sides by using the Low-Re release of the Wilcox  $k - \omega$  model while no-separation was predicted with  $k - \omega$  High-Re release. Due to the better agreement with experimental results the Low-Re formulation was selected as the reference model. It is interesting to note the improvements obtained with the formulation of the Wilcox  $k - \omega$  (2008) model as it is specifically tuned to better predict the shock-boundary layer interaction (note that  $k - \omega$  Low-Re and  $k - \omega$  (2008) curves are overlapped in fig. 4).

### Unsteady results

The numerical Schlieren visualization obtained with the GSC approach is displayed in fig. 5 at four different time instants. Results highlight the complex shock system present at 50% of the span height for the *High* pressure ratio. As can be easily seen, the direct shock *A* of the stator vane periodically interacts with the adjacent vane wake and impinges on the front part of the rotor SS. This interaction generates a reflected shock *D* that travels upstream reaching the vane SS. Here it is reflected downstream further on. Meanwhile a right running shock *B* strikes on the adjacent stator SS giving rise to reflections of variable strength. The intensity and the inclination of the shock change during the period due to the potential interaction with the rotor row. Finally the rotor left running trailing edge shock *C* is underlined in fig. 5. In the first snapshot it is rather weak while at the end of the rotor period it is enforced and reaches the neighboring blade suction side.

Fig. 6 displays the corresponding space-time plots at midspan for both the vane and the blade. The right running vane shock *B* is highlighted in the vane graph at a fixed position ( $s/s_{TOT} \sim 0.40$ ). At the same time the traces of the reflected shock *D* are fairly evident. Furthermore, the sweeping of the vane direct shock *A* from the crown to the LE of the blade is figured out as a space-time trace in the normalized pressure fluctuation of the rotor blade.

To better quantify the entity of unsteadiness over a period the pressure fluctuations have been stored

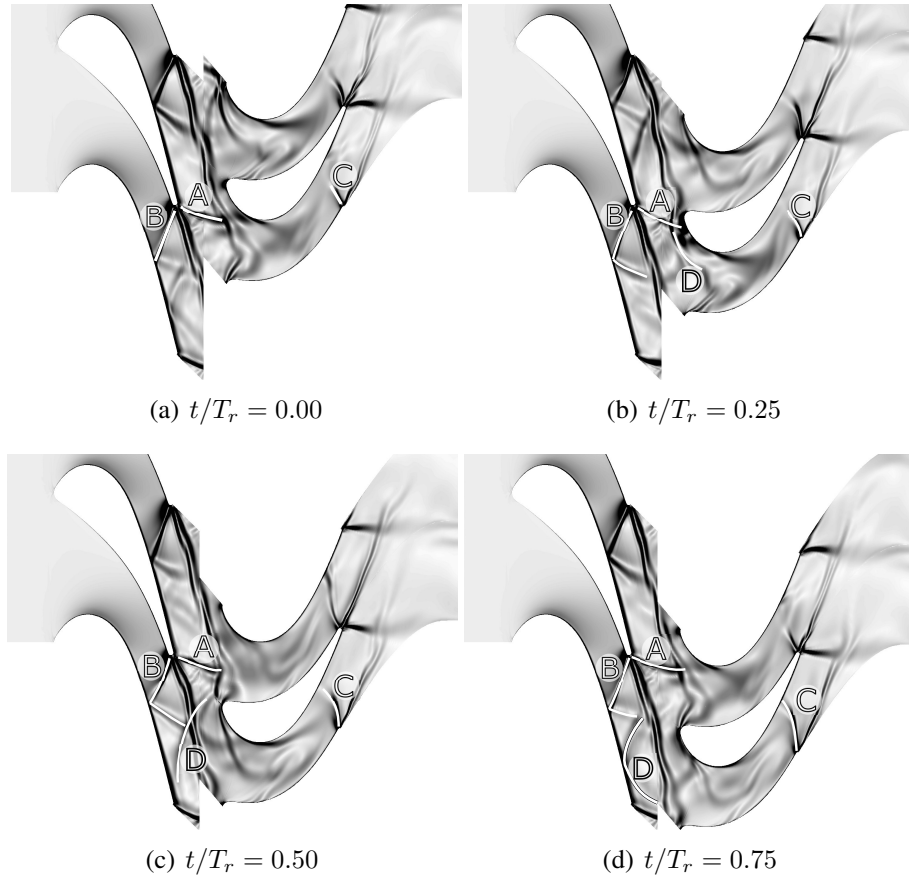


Figure 5: **3D unsteady (GSC) density gradient contours for the *High* pressure ratio (25% span).**

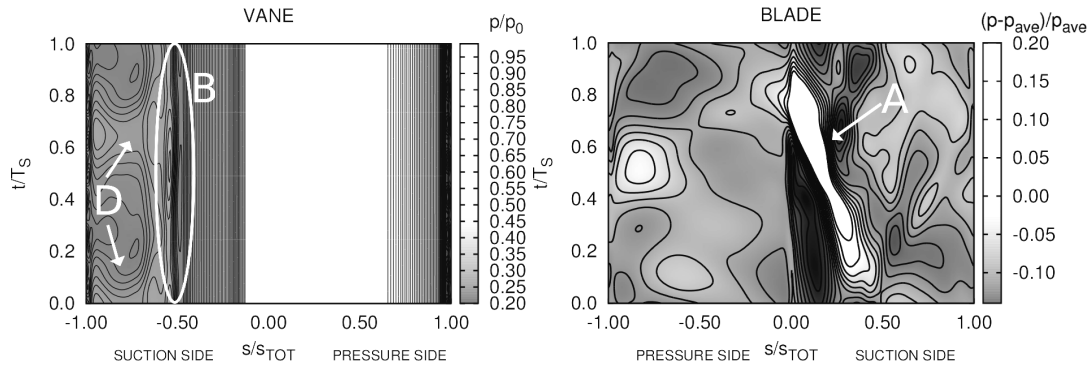


Figure 6: **Unsteady (GSC) pressure on the stator and the rotor blades (50% span)**

for every point of both the suction and the pressure sides of the stator and the rotor blades at midspan. The difference between the maximum and minimum pressure values normalized with the averaged one is plotted in fig. 7 in order to quantify the maximum pressure fluctuation over a period. The high level of unsteadiness in the rear part of the nozzle SS ( $\sim 20\%$  of the average pressure level) is due to both the motion of the right running shock *B* and the periodic impingement of the reflected shock branch *D*. On the rotor blade the maximum unsteadiness is detected around the leading edge as a results of the vane shock *A* impingement. On the first 30% of the rotor suction side the pressure field undergoes fluctuation of over the 100% of the mean values indicating the importance of correctly assessing the rotor-stator unsteady interaction. Fig. 8 reports the space-time plots of the

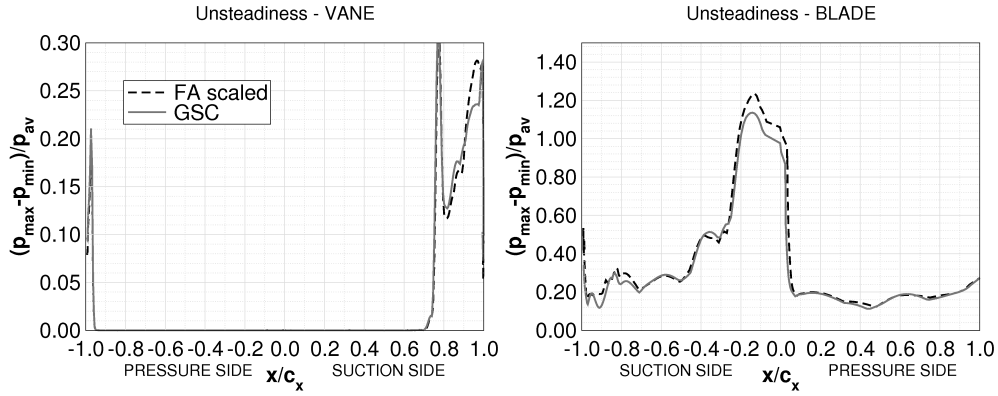


Figure 7: Unsteadiness on the vane and the blade surfaces at 50% of the blade span (*Nom cond.*)

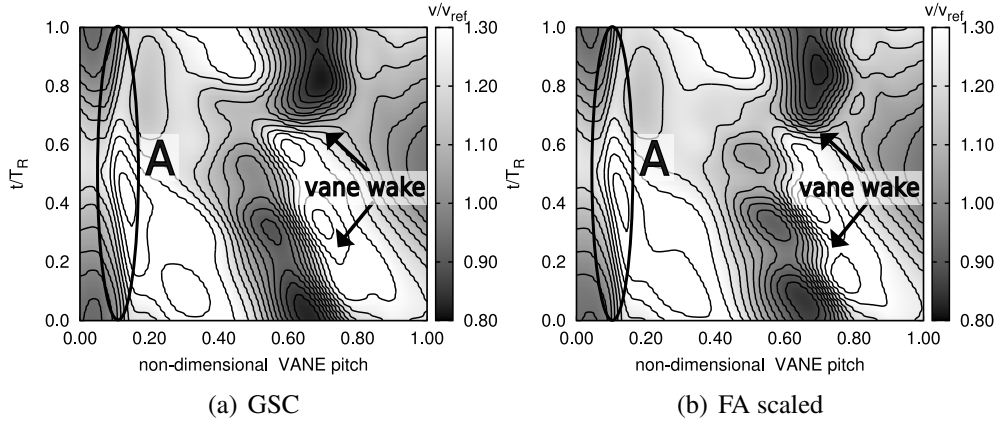


Figure 8: Time-space plots of the velocity magnitude (*Nom cond.*; plane 2, span 50%)

non-dimensional velocity magnitude computed in the vane-blade interface (plane 2) at midspan by using both the GSC and FA scaled approaches. Only one vane pitch is reported in the space coordinate while a single blade passing period is considered for the time one. On one hand this allow a direct comparison between the two models despite the fact that they solve different BPF, on the other hand the velocity contours are not periodic since the graphs does not cover a periodicity domain (neither in space nor in time). The direct shock *A* is highlighted in the two graphs as well as the vane wake trace. The direct shock *A* appears in a quite fixed position, while the vane blade interaction affects the shock intensity and induces considerable fluctuations of the vane wake. Finally, both fig. 7 and fig. 8 clearly show the good agreement among the GSC and the FA scaled results.

#### Time-averaged performance

Time averaged isentropic Mach number distributions obtained by means of the GSC approach are compared to experimental data in fig. 9. Results are plotted for both the stator and the rotor rows for the three investigated pressure ratios and show a good agreement with the experiments. The impingement of the right running shock of the vane on the adjacent SS causes the boundary layer separation. When the pressure ratio increases from the *Low* to the *Nom* conditions the shock results more inclined shifting downstream its impact with the neighbouring blade. The time-averaged vane load instead does not change from *Nom* to *High* conditions as the rotor row is choked and the vane exit Mach number remains the same. A second shock pattern is detected at the blade TE. The left running shock impinges on the adjacent blade affecting the time-averaged blade load at  $x/c_x \sim 0.7$  and  $x/c_x \sim 0.8$  for *Nom* and *High* conditions respectively.

The agreement with the experimental data is satisfactory and coherent with previous results already

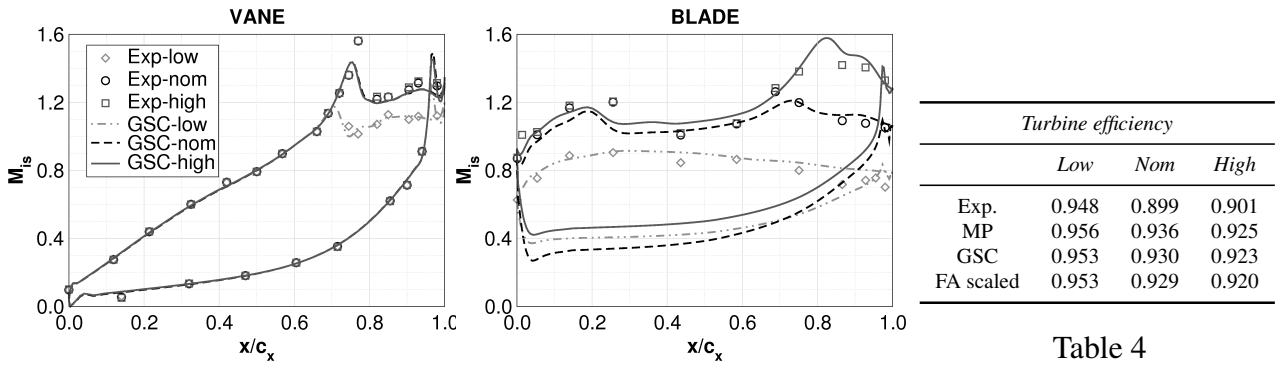


Figure 9: Time-averaged isentropic Mach number distribution on the stator and the rotor blades at midspan

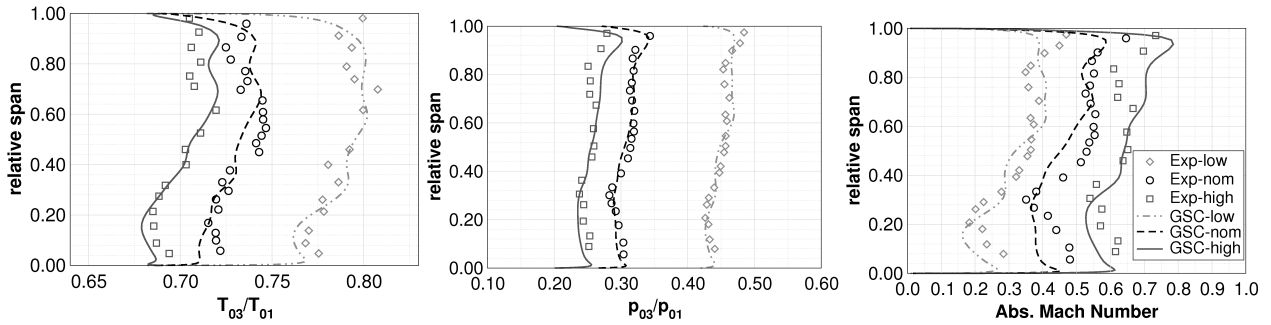


Figure 10: Time-averaged span-wise distr. on plane 3 ( $0.45 \cdot C_{x,R}$  downstream of the rotor TE)

presented in literature (De La Calzada and Fernandez-Castaneda (2003); Paniagua et al. (2008)). Fig. 10 reports the radial distributions of the time-averaged total temperature, total pressure, and Mach number in a plane located  $0.45 \cdot C_{x,R}$  downstream of the rotor TE. The numerical results show a good agreement with the experimental data, proving the accuracy of the numerical model adopted for the calculations. As far as overall turbine performance is concerned, tab. 4 reports the experimental and computed turbine efficiency. Results obtained with the three numerical approaches are very similar. However all of them miss to predict the correct efficiency variations among the three operating conditions. When the pressure ratio increases from the *Low* to *Nom* experiments suggest an efficiency reduction of 4.9 points while the computation predicts a smaller decrement ( $\sim 2$  points). Nevertheless similar discrepancies have been already reported and discussed in the available literature (Paniagua et al. (2008)). A further comparison among the different approaches MP, FA and GSC is

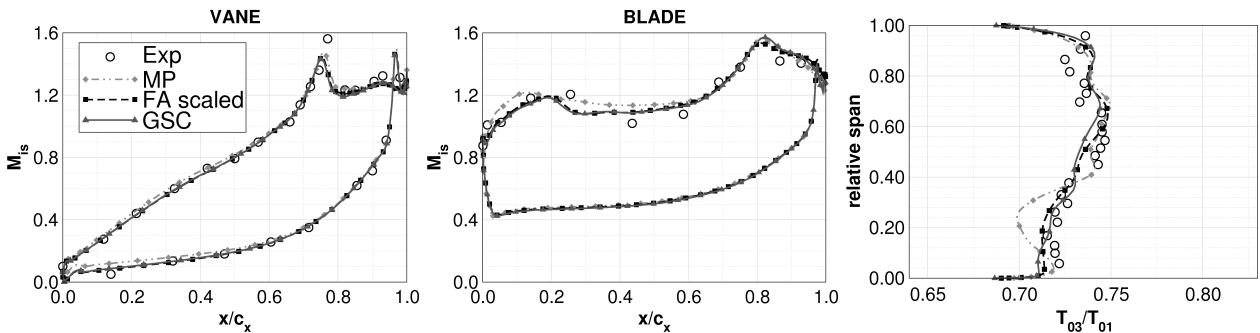


Figure 11: Comparison between steady and unsteady results (*Nom cond.*)

shown in fig. 11. As can be seen unsteady results match better the experimental data while no relevant differences can be found between FA and PL results proving that some main time-averaged performance parameter can be accurately predicted if a proper geometrical scaling is adopted. However, it is important to bear in mind that this “proper scaling” is not always possible and does not always lead to such relevant reduction of the computational domain.

## CONCLUSIONS

A Phase-Lagged method for unsteady turbomachinery applications was developed and validated. This model is based on the GSC approach and is able to accurately solve both single perturbation (rotor-stator interaction) and multi-stage problems. The numerical stability and robustness of the algorithm was substantially enhanced by the introduction of the two-passage approach. Despite the increased computational domain, the time-to-convergence was reduced to almost a fifth with respect to the original single-passage one.

The FA as well as the GSC models were applied to solve the high pressure transonic turbine stage CT3 and both their accuracy and computational costs were thoroughly evaluated. The FA approach with the real blade counts would provide the most accurate results, resolving the true spatial and frequency domain without any simplifying assumption. However, the detailed analysis of its computational costs clearly showed as its high memory ( $\sim 80\text{GB}$ ) and time ( $\sim 6000\text{CPU}$  hours) requirements practically prevent its daily adoption. In the FA scaled model a reduced domain with a 2:3 blade count ratio was considered with a pitch alterations of 2.4% and 1.6% for the stator and the rotor rows respectively. Time-averaged performance were accurately predicted with low computational costs but the main frequencies of the unsteady flow field were altered. The GSC results showed a fairly good agreement with the available experimental data. Moreover, the GSC model featured affordable memory ( $\sim 3\text{GB}$ ) and time ( $\sim 270\text{CPU}$  hours) requirements and allowed us to accurately investigate the unsteady rotor-stator interaction without any geometrical alteration. Such feature seems even more strategic as far as noise or vibrating issues are becoming more and more pressing and important for the turbomachinery industry. Therefore, the developed model appears certainly promising as an advanced tool of industrial interest for the analysis of large multi-stage problems (as whole LPT modules).

## ACKNOWLEDGMENTS

We would like to thank our fellow partners in European Union FP6 programme TATEF2 (Contract No. AST3-CT-2004-502924) for permitting the publication of our results in this paper.

## REFERENCES

- Adamczyk, J. J. (1985). Model equations for simulating flows in multistage-turbomachinery. In *ASME Conference Proceedings*, number GT85–226.
- Arnone, A. (1994). Viscous analysis of three-dimensional rotor flow using a multigrid method. *ASME J. Turbomach.*, 116(3):435–445.
- Arnone, A. and Pacciani, R. (1996). Rotor-stator interaction analysis using the navier-stokes equations and a multigrid method. *ASME J. Turbomach.*, 118(4):679–689.
- Barter, J. W., Vitt, P. H., and Chen, J. P. (2000). Interaction effects in a transonic turbine stage. In *ASME Conference Proceedings*, number 2000–GT–0376.
- Biesinger, T., Cornelius, C., Rube, C., Schmid, G., Braune, A., Campregher, R., Godin, P. G., and Zori, L. (2010). Unsteady CFD methods in a commercial solver for turbomachinery applications. In *ASME Conference Proceedings*, number GT2010–44021.
- Blumenthal, R., Hutchinson, B., and Zori, L. (2011). Investigation of transient CFD methods applied

- to a transonic compressor stage. In *ASME Conference Proceedings*. GT2011–46635.
- Chen, J. P. and Barter, J. W. (1998). Comparison of time-accurate calculations for the unsteady interaction in turbomachinery stage. *AIAA paper* 98-3292.
- De La Calzada, P. and Fernandez-Castaneda, J. (2003). Investigation of numerical and physical modelling effects on the CFD simulation of the unsteady flow in a hpt stage. *ASME Conference Proceedings*, 2003(36894):1175–1182.
- Dewhurst, S. and He, L. (2000). Unsteady flow calculations through turbomachinery stages using single-passage domain with shape-correction method. pages 338–350. 9<sup>th</sup> ISUAAAT, 4–8 September 2000, Lyon, France.
- Erdos, J. I., Alzner, E., and McNally, W. (1977). Numerical solution of periodic transonic flow through a fan stage. *AIAA Journal*, 15(11).
- Galpin, P. F., Broberg, R. B., and Hutchinson, B. R. (1995). Three-dimensional Navier Stokes predictions of steady state rotor/stator interaction with pitch change. In *Third Annual Conference of the CFD Society of Canada, June 25–27, Banff, Alberta, Canada*.
- Gerolymos, G. A. and Chapin, V. C. (1991). Generalized expression of chorochronic periodicity in turbomachinery blade-row interaction. *La Recherche Aéropatiale*, 5:69–73.
- Gerolymos, G. A., Michon, G. J., and Neubauer, J. (2002). Analysis and application of chorochronic periodicity in turbomachinery rotor/stator interaction computations. *Journal of Propulsion and Power*, 18(6):1139–1152.
- Giles, M. B. (1988). UNSFLO: A numerical method for unsteady inviscid flow in turbomachinery. Technical report, MIT Dept. of Aero. and Astro. GTL 195.
- Gopinath, A. K. (2007). *Efficient Fourier-Based Algorithms for time-periodic unsteady problems*. PhD thesis, Stanford University.
- Hall, K. C. and Ekici, K. (2005). Multistage coupling for unsteady flows in turbomachinery. *AIAA Journal*, 43(3):624–632.
- Hall, K. C. and Lorence, C. B. (1993). Calculation of three-dimensional unsteady flows in turbomachinery using the linearized harmonic Euler equations. *ASME J. Turbomach.*, 115:800–809.
- He, L. (1990). An Euler solution for unsteady flows around oscillating blades. *ASME J. Turbomach.*, 112:714–722.
- He, L. (1992). Method of simulating unsteady turbomachinery flows with multiple perturbations. *AIAA Journal*, 30(11):2730–22735.
- He, L., Chen, T., Wells, R. G., Li, Y. S., and Ning, W. (2002). Analysis of rotor-rotor and stator-stator interferences in multi-stage turbomachines. *ASME J. Turbomach.*, 124(4):564–571.
- He, L. and Ning, W. (1999). Nonlinear harmonic aerodynamic modelling. In *Lecture series programme on Aeroelasticity in axial flow turbomachines*. Von Karman Inst. for Fluid Dynamics.
- Li, H. D. and He, L. (2001). Single-passage solution of three-dimensional unsteady flows in a transonic fan rotor. *Journal of Power and Energy*, 215:653–662.
- Loma, A. D. L., Paniagua, G., Verrastro, D., and Adami, P. (2007). Transonic turbine stage heat transfer investigation in presence of strong shocks. *ASME Conference Proceedings*, 2007(47950):1563–1573.
- Neubauer, J. (2004). *Aérodynamique 3-D Stationnaire des Turbomachines Axiales Multi-Étages*. PhD thesis, Université Paris 6.
- Pacciani, R., Marconcini, M., Fadai-Ghotbi, A., Lardeau, S., and Leschziner, M. A. (2011). Calculation of high-lift cascades in low pressure turbine conditions using a three-equation model. *ASME J. Turbomach.*, 133(3).
- Paniagua, G., Yasa, T., Loma, A. D. L., and Coton, T. (2008). Unsteady strong shock interactions

- in a transonic turbine: Experimental and numerical analysis. *Journal of Propulsion and Power*, 24(4):722–731.
- Spalart, P. R. and Allmaras, S. R. (1994). A one–equation turbulence model for aerodynamic flows. *La Recherche Aéronautique*, 1:5–21.
- Van Zante, D., Chen, J., Hathaway, M., and Chriss, R. (2008). The influence of compressor blade row interaction modeling on performance estimates from time–accurate, multistage, navier–stokes simulations. *ASME J. Turbomach.*, 130(1):011009.
- Vilmin, S., Larrain, E., Hirsch, C., and Swoboda, M. (2006). Unsteady flow modeling across the rotor/stator interface using the nonlinear harmonic method. (GT2006–90210).
- Wilcox, D. C. (1998). *Turbulence Modeling for CFD*. DCW Industries Inc., La Cañada, CA, USA, 2<sup>nd</sup> edition. ISBN 1-928729-10-X.
- Wilcox, D. C. (2008). Formulation of the  $k - \omega$  turbulence model revisited. *AIAA Journal*, 46(11):2823–2838.